Publisher's PDF, also known as Version of record

Link to publication record in Explore Bristol Research
PDF-document

University of Bristol - Explore Bristol Research
General rights

Silicon photonic 8 × 8 cyclic Arrayed Waveguide Grating Router for O-band on-chip communication

STELIOS PITRIS,[1,2,*] GEORGE DABOS,[1,2] CHAROULA MITSOLIDOU,[1,2] THEONI ALEXOUDI,[1,2] PETER DE HEYN,[3] JORIS VAN CAMPENHOUT,[3] RONALD BROEKE,[4] GEORGE T. KANELLOS,[5] AND NIKOS PLEROS[1,2]

[1]Department of Informatics, Aristotle University of Thessaloniki, Thessaloniki, 54124, Greece
[2]Center for Interdisciplinary Research and Innovation, Aristotle University of Thessaloniki, Thessaloniki, 57001, Greece

[3]imec, Kapeldreef 75, Leuven B-3001, Belgium
[4]Bright Photonics B.V., Horsten 1, 5621 AX Eindhoven, The Netherlands
[5]High Performance Networks Group, University of Bristol, Bristol, United Kingdom
*skpitris@csd.auth.gr

Abstract: We report an 8 × 8 silicon photonic integrated Arrayed Waveguide Grating Router (AWGR) targeted for WDM routing applications in O-band. The AWGR was designed for cyclic-frequency operation with a channel spacing of 10 nm. The fabricated AWGR exhibits a compact footprint of 700×270 μm^2. Static device characterization revealed 3.545 dB maximum channel loss non-uniformity with 2.5 dB best-case channel insertion losses and 11 dB channel crosstalk, in good agreement with the simulated results. Successful data routing operation is demonstrated with 25 Gb/s signals for all 8 × 8 AWGR port combinations with a maximum power penalty of 2.45 dB.

References and links

1. N. Binkert, A. Davis, N. P. Jouppi, M. McLaren, N. Muralimanohar, R. Schreiber, and J. H. Ahn, "The role of optics in future high radix switch design," in *Proceedings 38th Annual International Symposium on Computer Architecture (ISCA)*, 437–447 (2011).
2. S. Papaioannou, G. Giannoulis, K. Vyrsokinos, F. Leroy, F. Zacharatos, L. Markley, J. C. Weeber, A. Dereux, S. I. Bolzhevolnyi, A. Prinzen, D. Apostolopoulos, H. Avramopoulos and N. Pleros, "Ultra-compact and low-power plasmonic MZI switch using Cyclomer loading," IEEE Photonics Technol. Lett. **27**(9), 963–966 (2015).
3. A. Rosa, A. Gutiérrez, A. Brimont, A. Griol, and P. Sanchis, "High performace silicon 2x2 optical switch based on a thermo-optically tunable multimode interference coupler and efficient electrodes," Opt. Express **24**(1), 191–198 (2016).
4. D. Nikolova, S. Rumley, D. Calhoun, Q. Li, R. Hendry, P. Samadi, and K. Bergman, "Scaling silicon photonic switch fabrics for data center interconnection networks," Opt. Express **23**(2), 1159–1175 (2015).
5. H. Liu, C. F. Lam, and C. Johnson, "Scaling optical interconnects in datacenter networks - opportunities and challenges for WDM," in *Proceedings 18th High Performance Interconnects Conference*, 113–116 (2010).
6. X. Leijtens, M. J. B. Kuhlow, and M. K. Smit, "Arrayed waveguide gratings," in *Wavelength Filters in Fiber Optics*, H. Venghaus, ed. (2006).
7. D. A. B. Miller, "Device Requirements for Optical Interconnects to Silicon Chips," in *Proceedings of the IEEE*, (IEEE, 2009), pp. 1166–1185.
8. A. A. M. Saleh, A. S. P. Khope, J. E. Bowers, and R. C. Alferness, "Elastic WDM Switching for Scalable Data Center and HPC Interconnect Networks", in *Proceedings of OECC* (2016), pp. 1–3.
9. R. Proietti, Z. Cao, Y. Li, and S. J. B. Yoo, "Scalable and distributed optical interconnect architecture based on AWGR for HPC and data centers," in *Proceedings Optical Fiber Communication Conference*, OSA Technical Digest Series (Optical Society of America, 2014), paper Th2A.59.
10. R. Yu, S. Cheung, Y. Li, K. Okamoto, R. Proietti, Y. Yin, and S. J. B. Yoo, "A scalable silicon photonic chip-scale optical switch for high performance computing systems," Opt. Express **21**(26), 32655–32667 (2013).
11. P. Grani, R. Proietti, S. Cheung, and S. J. B. Yoo, "'Flat-Topology High-Throughput Compute Node With AWGR-Based Optical-Interconnects," J. Lightwave Technol. **34**(12), 2959–2968 (2016).
12. G. T. Kanellos and N. Pleros, "WDM mid-board optics for chip-to-chip wavelength routing interconnects in the H2020 ICT-STREAMS," Proc. SPIE **10109**, 101090D (2017).

13. J. Wang, Z. Sheng, L. Li, A. Pang, A. Wu, W. Li, X. Wang, S. Zou, M. Qi, and F. Gan, "Low-loss and low-crosstalk 8 × 8 silicon nanowire AWG routers fabricated with CMOS technology," Opt. Express **22**(8), 9395–9403 (2014).
14. N. A. Idris and H. Tsuda, "6.4-THz-spacing, 10-channel cyclic arrayed waveguide grating for T- and O-band coarse WDM," IEICE Electron. Express **13**(7), 1–7 (2010).
15. M. Zirngibl, C. Dragone, and C. H. Joyner, "Demonstration of a 15x15 arrayed waveguide multiplexer on InP," IEEE Photonics Technol. Lett. **4**(11), 1250–1253 (1992).
16. S. Takenobu, Y. Kuwana, K. Takayama, Y. Sakana, M. Ono, H. Sato, N. Kiel, W. Brinker, H. Yao, C. Zawadzki, Y. Morizawa, and N. Grote, "All-polymer 8x8 AWG Wavelength Router using Ultra Low Loss Polymer Optical Waveguide Material (CYTOPTM)," in *Proceedings Optical Fiber Communication Conference/National Fiber Optic Engineers Conference*, OSA Technical Digest Series (Optical Society of America, 2008), pp. 1–3.
17. D. Seyringer, "Arrayed Waveguide Gratings," in *SPIE Spotlight Publications*, (SPIE, 2016).
18. P. Dumon, W. Bogaerts, D. Van Thourhout, G. Mortier, and R. Baets, "A Nanophotonic 4x4 Wavelength Router in Silicon-on-Insulator," in *Proceedings Optical Fiber Communication Conference and Exposition and The National Fiber Optic Engineers Conference*, OSA Technical Digest (CD) (Optical Society of America, 2006), paper OThO5.
19. Y. Chen, J. Zou, T. Lang, and J. He, "SOI-based Arrayed Waveguide Grating Router with grating couplers fabricated in a single shallow etching step," in *Proceedings Asia Communications and Photonics Conference*, OSA Technical Digest (Optical Society of America, 2015), paper ASu2A.22.
20. S. Pathak, M. Vanslembrouck, P. Dumon, D. Van Thourhout, and W. Bogaerts, "Compact 16x16 Channels Routers Based on Silicon-on-insulator AWGs," in *Proceedings of Annual Symposium of the IEEE Photonics Benelux Chapter (IEEE,2011)*, pp. 101–104.
21. S. Cheung, T. Su, K. Okamoto, and S. J. B. Yoo, "Ultra-Compact Silicon Photonic 512 × 512 25 GHz Arrayed Waveguide Grating Router,'," IEEE J. Sel. Top. Quantum Electron. **20**(4), 310–316 (2014).
22. G. Chen, J. Zou, T. Lang, and J. He, "Compact 4×4 1250 GHz silicon arrayed waveguide grating router for optical interconnects," Proc. SPIE **9367**, 936717 (2015).
23. G. Song, J. Zou, and J. He, "Ultra-compact silicon-arrayed waveguide grating routers for optical interconnect systems," Chin. Opt. Lett. **15**(3), 030603 (2017).
24. *100G–CLR4 Alliance, "Specification for 100 Gb/s Coarse Wavelength Division Multiplex Optical Data Transmission",* https://www.clr4-alliance.org/media/doc/100G-CLR4-Specification_v1p52_FINAL
25. *Bright Photonics B. V.,* http://brightphotonics.eu/
26. E. J. Stanton, N. Volet, and J. E. Bowers, "Low-loss demonstration and refined characterization of silicon arrayed waveguide gratings in the near-infrared," Opt. Express **25**(24), 30651–30663 (2017).
27. M. K. Smit and C. Van Dam, "PHASAR-based WDM-devices: Principles, design and applications," IEEE J. Sel. Top. Quantum Electron. **2**(2), 236–250 (1996).

1. Introduction

Ware-house datacenters and high-performance computers (HPC) are constantly scaling up, imposing new requirements for high-capacity networks to exhibit low-latency, high-throughput and low-power links. Optical interconnects have emerged as the key enabling technology for deploying point-to-point high-bandwidth links and pressure is now put also in the switching and routing elements to handle the massive throughput enabled by the optical links. Recent attempts are focusing on taking advantage of the progress in photonic integration towards producing alternative on-chip switching and routing schemes that can reap the inherent speed and energy benefits of optics [1–4]. In this context, wavelength routing based on Arrayed Waveguide Gratings Routers (AWGRs) has emerged as a promising interconnection solution for datacom environments [5], since AWGRs can offer a low latency, non-blocking interconnection even for an all-to-all communication scheme, when employed as N × N routers [6]. AWGRs are completely passive devices allowing for routing to be performed directly in the optical domain without consuming additional energy. They have been already successfully employed at every level of Datacom interconnect hierarchy [7], extending from rack-to-rack interconnects [8], through board-level chip-to-chip interconnects [9] down to on-chip routing layouts [10], demonstrating important benefits in terms of network expandability, network flattening [11] and multi-socket computing performance [12].

So far, AWGRs have been demonstrated as integrated devices in a great variety of integration platforms such as silicon [13], silica [14], InP [15], polymer [16]. Though low-index materials have managed to demonstrate high-quality devices reaching

commercialization maturity, silicon photonics integration can provide high-index-contrast AWGRs leading to smaller waveguide bending radius and reduced device size down to μm²-scale [17]. Moreover, silicon photonics CMOS-compatible technology processes may allow for large-scale integration of AWGRs along with other Si-based devices in a single photonic chip.

A C-band 4 × 4 AWGR in SOI with 250 GHz spacing and 3.5 dB insertion losses has been demonstrated in [18], while 8 × 8 [19] and 16 × 16 [20] AWGRs with 200 GHz and 400 GHz channel spacing configurations have also been demonstrated, exhibiting insertion losses of 1.9 dB and 3 dB, respectively. AWGRs with higher port count, up to 512 × 512, for DWDM routing have also been shown in SOI [21] with 25 GHz channel spacing, designed for operation in S-, C- an L-bands. AWGRs based on silicon-nanowires with 4 × 4 [22,23] and 8 × 8 [13] configurations have been demonstrated also, aiming to reduce the total footprint of the device. However, no Si-based AWGR structure has been deployed so far for O-band operation and all silicon photonic AWGRs have been demonstrated only as C-band operational units, despite O-band comprises a highly attractive and strongly utilized spectral region in the interconnect application area.

In this paper, we present for the first time, to our knowledge, a silicon photonic 8 × 8 AWGR on-chip router that operates in the O-band and has a low-footprint of 700 × 270 μm². The AWGR center wavelengths are aligned to partially match the 100G CWDM center wavelength specifications [24], having 10 nm channel spacing, 5.7 nm 3-dB bandwidth and a free spectral range (FSR) of 80 nm. The device exhibits proper cyclic frequency properties for all 8 × 8 port combinations with channel insertion losses ranging from 2.5 dB to 6.045 dB and a maximum power loss non-uniformity of 3.545 dB among all port combinations. The channel crosstalk was measured to be 11 dB. The AWGR chip was also evaluated experimentally with respect to its data routing performance using 25 Gb/s PRBS7 signals, revealing successful performance for all 8 × 8 channel combinations with a maximum power penalty of 2.45 dB. A comparison of the basic characteristics between the AWGR in this work and previous AWGR demonstrations in different spectral bands and integration platforms can be found in Table 1 below.

Table 1. Comparison between state-of-the-art AWGRs

	Band	Port count	Platform	Ch. Spacing		Ins. losses	Xtalk	Device Size
[10]	C	8 × 8	Si	1.6 nm (200 GHz)	DWDM	9 dB	13 dB	0.5 × 0.6 mm²
[13]	C-band	8 × 8	Si	0.8 nm (100 GHz)	DWDM	2.92 dB	16.9 dB	-
[14]	T-/O-band	10 × 10	Silica	28.2 nm (6.4 THz)	CWDM	6.4-8.4 dB	30 dB	30 × 65 mm²
[15]	C-band	15 × 15	InP	0.7 nm (87 GHz)	DWDM	2-7 dB	18 dB	10 × 10 mm²
[16]	C-band	8 × 8	Pol	1.6 nm (200 GHz)	DWDM	2.5-3.9 dB	25 dB	14.5 × 45 mm²
[18]	C-band	4 × 4	Si	2 nm (250 GHz)	DWDM	3.5 dB	12 dB	0.4 × 0.15 mm²
[20]	C-band	16 × 16	Si	3.2 nm (400 GHz)	DWDM	3-5.09 dB	19 dB	0.475 × 0.33 mm²
[21]	C-/S-/L- bands	512 × 512	Si	0.2 nm (25 GHz)	DWDM	-	4 dB	16 × 11 mm²
[22]	C-band	4 × 4	Si	10 nm (1.25 THz)	CWDM	2.5-5.5 dB	18 dB	0.46 × 0.26 mm²
[23]	C-band	4 × 4	Si	20 nm (2.5 THz)	CWDM	2.5 dB	20 dB	0.27 × 0.19 mm²
This work	O-band	8 × 8	Si	10 nm (1.77 THz)	CWDM	2.5-6 dB	11 dB	0.7 × 0.27 mm²

2. Principle of operation, design and fabrication

The cyclic frequency operation in a 4 × 4 AWGR is depicted in Fig. 1(a). When a set of WDM signals (λ_{ix}; where i is the input port number and x is the wavelength indicator) is inserted to each one of the four inputs ports of the AWGR, they are routed to the output ports based on their wavelength characteristics. The wavelength mapping of the incoming signals from all input ports to the output ports of the AWGR can be seen in Fig. 1(a). The cyclic-frequency property of the AWGR can be verified by tracking down the relative rotation of the wavelength sets originating from each input port that emerge shifted at neighboring output

channels of the AWGR. In this way, a N × N AWGR supports N^2 interconnections when employed as N × N router in an interconnect architecture, requiring the use of N wavelengths.
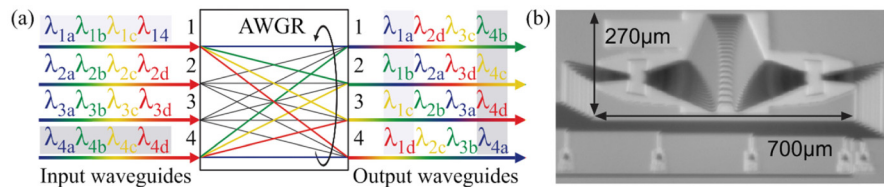

Fig. 1. (a) Cyclic frequency operation in a N × N AWGR (N = 4). (b) Microscope image of the fabricated 8 × 8 AWGR.

Table 2. Main design parameters of the 8 × 8 AWGR

Parameter	Design value
Port count	8 × 8
Center wavelength	1301 nm
Channel spacing	10 nm
Peak wavelengths	1261, 1271, 1281, 1291, 1301, 1311, 1321, 1331 nm
3-dB bandwidth	5.7 nm
Free spectral range	80 nm
Peak deviation	< 6 nm

The AWGR presented in this paper was designed by means of the Bright Photonics *BrightAWG* toolkit [25] for operation in the O-band for a center wavelength at 1301 nm, targeting a 10-nm channel spacing in order to partially match with the 100G CWDM channel specification but with a denser (8 × 8) channel configuration. The AWGR was designed with a targeted 3-dB channel bandwidth of 5.7 nm, a free spectral range of 80 nm and passband peak deviation of below 6 nm. The main design characteristics of the reported 8 × 8 AWGR are summarized in Table 2.

The fabrication of the integrated AWGR relied on the imec-ePIXfab silicon photonics passives technology using a 220 nm-thick Si and 2 μm-thick buried oxide layer (SOI). A side and top oxide cladding was used. With three different (220 nm, 150 nm and 70 nm) Si etch depths layers, this technology allows for various passive integrated photonic components, such as strip waveguides, rib waveguides, fiber couplers and multi-mode interferometers, on the same chip. Figure 1(b) shows a microscope image of the fabricated AWGR with part of the I/O waveguide configuration. Fiber grating couplers (GC), with a 70 nm etch depth and a peak wavelength at 1285 nm, were used to couple the light in and out the integrated chip. The GCs were arranged with 250 μm pitch for probing the integrated photonic chip through a 16-channel Fiber Array (FA). The dimensions of the fabricated AWGR were 700 × 270 μm².

3. Simulation and experimental characterization

The simulated spectral response for all port combinations of the AWGR can be seen in Fig. 2. The AWGR channel spectral responses were simulated as Gaussian approximations to estimate the insertion losses, channel loss non-uniformity, 3 dB-bandwidth and channel peak wavelengths. The simulated channel peak wavelengths of the 8 input channels of the AWGR channels are shown in Table 3 respectively. The simulated 3 dB-bandwidth of the channels is 5.7 nm while the simulated channel crosstalk was >20 dB, respectively. The simulated peak losses of the channels are included in Table 3 along with the minimum losses (Min), maximum losses (Max) and loss non-uniformity (Uni) for each input port combination. The channel losses range from 1.198 dB to 3.255 dB with a maximum loss non-uniformity of 2.057 dB, defined as the difference between the maximum and minimum channel losses. Figure 3(a) shows the experimental setup employed for the characterization of the fabricated device. To test the 8 × 8 AWGR chip, a 16-channel fiber array with 250 μm pitch was used to

probe the chip through the respective GCs operating at a 6.9° angle. A tunable laser source (TLS)
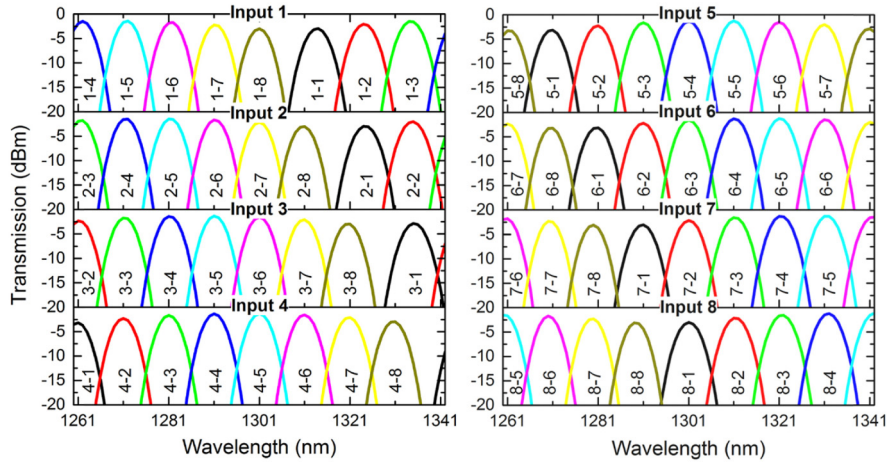

Fig. 2. Simulated spectral response of the 8 × 8 AWGR channels.

Table 3. Simulated channel peak wavelengths and insertion losses for all 8 × 8 AWGR port combinations

		Out1	Out2	Out3	Out4	Out5	Out6	Out7	Out8	Min	Max	Uni
In1	nm	1314	1324	1334	1262	1272	1282	1291	1301			
	dB	2.981	2.062	1.536	1.470	1.446	1.752	2.219	3.010	1.446	3.007	1.561
In2	nm	1324	1335	1262	1272	1281	1291	1301	1311			
	dB	2.969	2.029	1.806	1.525	1.455	1.642	2.147	3.010	1.455	3.010	1.555
In3	nm	1335	1261	1271	1281	1291	1301	1311	1321			
	dB	2.887	2.342	1.737	1.409	1.355	1.586	2.125	3.010	1.355	3.007	1.652
In4	nm	1261	1271	1281	1291	1301	1311	1321	1331			
	dB	3.175	2.268	1.667	1.350	1.309	1.550	2.089	2.960	1.309	3.175	1.866
In5	nm	1271	1281	1291	1301	1311	1321	1331	1261			
	dB	3.164	2.236	1.627	1.309	1.270	1.508	2.034	3.250	1.270	3.255	1.985
In6	nm	1281	1291	1301	1311	1321	1331	1261	1271			
	dB	3.131	2.193	1.586	1.277	1.247	2.313	2.313	3.210	1.247	3.212	1.965
In7	nm	1291	1301	1311	1321	1332	1261	1270	1280			
	dB	3.064	2.147	1.571	1.299	1.276	1.790	2.320	3.100	1.276	3.098	1.822
In8	nm	1301	1311	1322	1332	1260	1270	1280	1289			
	dB	3.007	2.160	1.556	1.198	1.534	1.713	2.272	3.100	1.198	3.100	1.901

for O-band (Yenista T100S-HP) was used for the characterization in combination with a polarization controller (PC) to verify that TE polarization was launched each time onto 1 of the 8 FA ports leading to the GCs that correspond to the 8 inputs of the AWGR, respectively. The 8 FA ports corresponding to the 8 outputs of the AWGR were connected to an 8-channel optical power meter (Agilent N7745A) to obtain the spectral response of all channels. The spectral response obtained for all 8 × 8 port combinations of the AWGR is shown in Fig. 3(b). The measured transmission graphs were produced after extracting all the estimated fiber losses, waveguide transmission losses and grating coupler losses for the transmission link.

Reference straight waveguides were also included in the chip layout for normalizing the AWGR transmission spectra based on the waveguide normalization method. The standard uncertainty in the measured AWGR insertion loss values was calculated to be ~7.93% (based on 12 waveguides), as described in [26]. The grating coupler losses were measured to be 4 dB/GC while the input/output FA losses were calculated to be 2 dB. The spectral response of the AWGR channels indicates proper cyclic-frequency operation that can be verified by the

same-colored output responses for each one of the different input ports. Table 4 presents the peak wavelengths of all input channels measured for all AWGR port combinations. The measured peak wavelengths
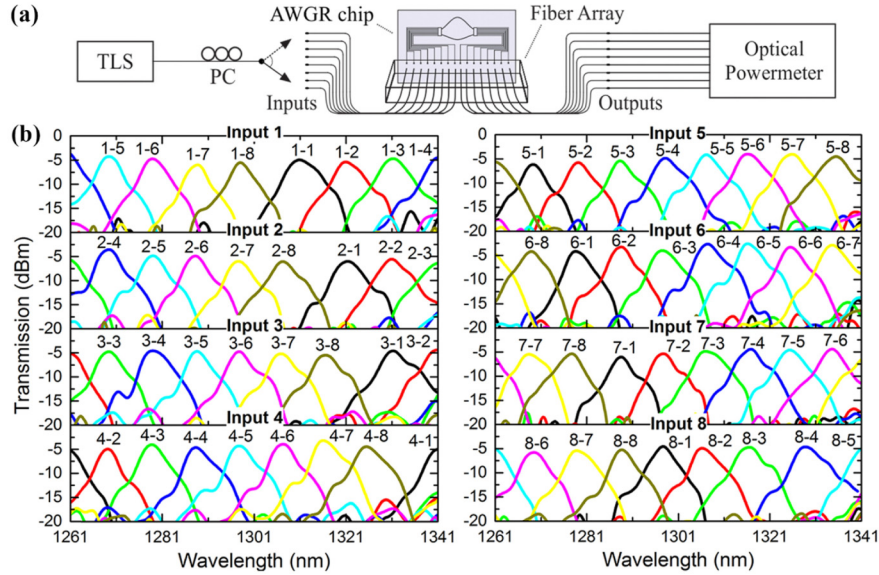

Fig. 3. (a) Experimental setup used for the characterization of the 8 × 8 AWGR. (b) Measured spectral response of the 8 × 8 AWGR channels.

Table 4. Measured channel peak wavelengths and peak insertion losses for all 8 × 8 port combinations.

		Out1	Out2	Out3	Out4	Out5	Out6	Out7	Out8	Min	Max	Uni
In1	nm	1310.9	1320.9	1331.3	1260	1269.4	1278.9	1288.7	1298			
	dB	4.952	5.373	4.705	3.189	4.248	4.737	5.989	5.533	3.189	5.989	2.800
In2	nm	1321.4	1331	1260.3	1269.4	1279	1288.2	1297.6	1307.2			
	dB	6.016	5.554	5.585	3.586	4.857	4.909	6.005	6.045	3.586	6.000	2.400
In3	nm	1331.2	1260	1269.4	1278.9	1288.5	1297.7	1306.9	1316.5			
	dB	4.586	5.000	4.761	4.559	4.688	4.742	5.192	5.483	4.559	5.483	0.925
In4	nm	1260.1	1269.2	1278.7	1288.3	1297.8	1307.3	1316	1325.4			
	dB	4.914	4.951	4.043	4.620	4.298	3.933	3.178	4.454	3.178	4.951	1.773
In5	nm	1269.2	1279.1	1288.3	1298.1	1307.1	1316.1	1325.9	1260			
	dB	4.900	5.773	5.430	4.859	4.147	4.010	4.052	5.256	4.010	5.773	1.763
In6	nm	1278.6	1288.5	1297.5	1307.4	1316.1	1325.5	1260.1	1268.9			
	dB	4.173	3.263	4.007	2.500	2.567	3.317	4.200	4.201	2.500	4.201	1.700
In7	nm	1288.5	1297.7	1306.9	1316.9	1325.4	1260.2	1268.3	1277.7			
	dB	6.027	5.360	4.857	4.409	4.603	5.400	5.475	5.374	4.409	6.027	1.618
In8	nm	1297.7	1306.2	1316.5	1328.8	1260.5	1269.4	1278.8	1288.7			
	dB	4.549	4.924	4.721	4.629	4.925	5.788	5.412	5.238	4.549	5.788	1.239

of the device were on average at 1260.15 nm, 1269.15 nm, 1278.71 nm, 1288.46 nm, 1297.76 nm, 1307.49 nm, 1317.55 nm and 1328.06 nm (herein referred to as the AWGR mean wavelengths). The AWGR channel peak wavelengths exhibited a standard deviation of 0.177, 0.385, 0.439, 0.185, 0.200, 1.428, 2.245, 2.801 nm, respectively. The mean wavelengths were calculated each time as the mean value among the channel peak wavelengths belonging to the same diagonal of Fig. 3(b) that correspond to the same AWGR resonance. The 3 dB-bandwidth of the channels was measured to be 5.5 nm. The measured channel peak losses are included in Table 4 along with the minimum losses (Min), maximum losses (Max) and loss

non-uniformity (Uni) for each input port comb. The measured channel peak losses range from 2.5 dB to 6.045 dB, indicating a maximum loss non-uniformity of 3.545 dB for the fabricated device. The measured channel crosstalk was measured to be 11 dB on average, while the mean 3dB-cumulative crosstalk (3dB-CXT) per channel [26] was calculated to be 6.019 dB with a standard deviation of 0.331. The difference in the channel shape between the measured and the simulated AWGR spectral responses originates to the Gaussian approximations of the simulated AWGR channels that do not take into account various crosstalk mechanisms as described in [27].

4. 8 × 8 Data Routing Operation
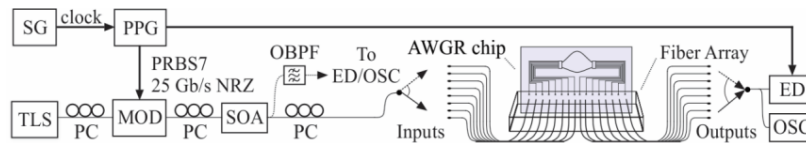

Fig. 4. Experimental setup used for the data routing operation at 25 Gb/s.

The AWGR was used to demonstrate data routing operation at 25 Gb/s in an 8 × 8 configuration. The experimental setup used for the demonstration is shown in Fig. 4. A signal generator (SG) was used to drive a programmable pattern generator (PPG) at 25 GHz. The PPG was used to drive the $LiNbO_3$ modulator in order to produce the 25 Gb/s PRBS7 NRZ signals at different wavelengths. A TLS was used to provide all wavelengths within the operational range of the AWGR according to Table 4. The modulated signals were amplified by a semiconductor optical amplifier (SOA) with 32 dB small signal gain and amplified spontaneous emission (ASE) peak wavelength at 1300.3 nm and were then launched to the AWGR through the respective FA ports. The routed signals were collected at the respective FA output ports with respect to their wavelength and were collected by an error detector (ED) and a digital sampling oscilloscope (OSC). Polarization controllers (PC) were employed at different stages of the setup to maintain proper signal polarization. An optical bandpass filter (OBPF) with 2.5 nm 3 dB-bandwidth was used at the SOA output to obtain the back-to-back (B2B) measurements and eye diagrams.

The device was initially tested for data routing in an 8 × 8 configuration with the TLS emitting each time at one of the AWGR channel peak wavelengths, so that finally a total number of 64 wavelength values had to be used in order to optimally align on all AWGR resonances. Successful data routing operation was achieved at 25 Gb/s with error-free transmission through all 8 × 8 port combinations. Figure 5(a) depicts the BER curves for data transmission at 25 Gb/s for Input 1 to all 8 output ports, while Fig. 5(b) shows the BER curves for all 8 Input ports to Output 1, respectively. A maximum power penalty of 0.58 dB and 0.63 dB was observed for the two BER curves, respectively, for an error-rate value of 10^{-9}. Figures 5(c) and 5(d) depict the eye diagrams of the PRBS7-modulated signal at 1288.7 nm, at the input and at the output of the AWGR with transmission through Input 1 and Output 8 ports, respectively. The eye diagrams exhibit an extinction ratio of 6.9 dB and 6.85 dB, respectively. Finally, Table 5(a) shows the power penalty values obtained for transmission through all possible 8 × 8 port combinations at a BER value of 10^{-9}, indicating a maximum power penalty of 0.82 dB.

Towards evaluating its performance in a realistic application scenario where a fixed identical set of 8 wavelength channels will be employed at every transmitting node connected to every AWGR input port, the AWGR was tested for 8 × 8 data routing using a fixed set of 8 different wavelengths. The TLS was used to generate each time one of the 8 wavelengths launched in each one of the AWGR inputs. These 8 wavelengths were selected to coincide with the AWGR mean wavelength values, which equal the mean among the peak wavelength values of the same AWGR resonance emerging at all its output ports, i.e. 1260.15 nm, 1269.15 nm, 1278.71 nm, 1288.46 nm, 1297.76 nm, 1307.49 nm, 1317.55 nm and 1328.06

nm, respectively. Successful data routing was achieved for transmission of 25 Gb/s optical signals at all 8 wavelength channels and in all possible input/output port combinations, revealing a maximum power penalty of 2.45 dB. The additional power penalties for transmission at channel peak wavelengths versus transmission at the fixed set of the 8 mean wavelengths for all port combinations for an error-rate of 10^{-9} can be found in Table 5(b). Table 6(a) shows the deviation of the mean wavelengths compared with the respective AWGR optimal resonances, while Table 6(b) shows the mean wavelength values with their respective standard deviation and range values between the mean wavelengths and the AWGR optimal resonances. In the case of transmission through AWGR channels with higher standard deviation from the respective mean wavelength, increased power penalty values are observed due to signal distortion. The TLS was set to 10 dBm output power for all wavelengths while the SOA was driven at a driving current of 660 mA for all measurements.
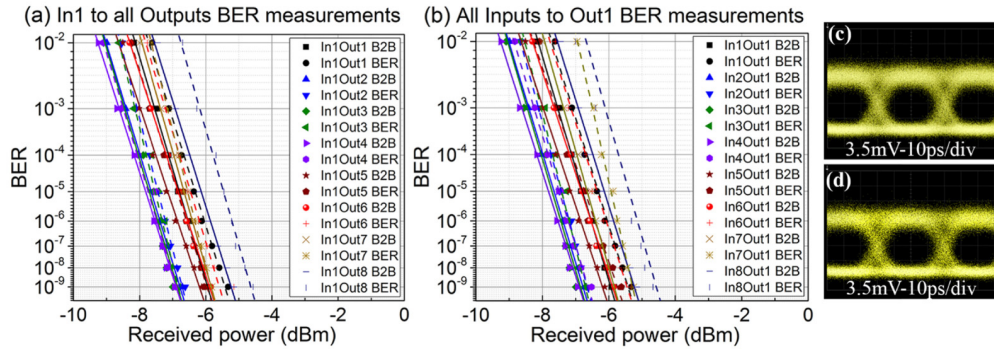

Fig. 5. BER measurements for transmission through (a) In1 to all output ports, (b) All input ports to Out1. Eye diagram of 25 Gb/s PRBS7-modulated signal at 1288.7 nm (c) at the input of the AWGR and (d) at the output of the AWGR after transmission through ports In1 Out7.

Table 5. (a) Power penalty values (dB) for data routing at 25 Gb/s for transmission at AWGR peak wavelengths. (b) Additional power penalty on top of the power penalty of the first scenario when transmitting at the mean wavelengths.

(a)

db	Out1	Out2	Out3	Out4	Out5	Out6	Out7	Out8
In1	0.60	0.09	0.17	0.04	0.07	0.31	0.08	0.58
In2	0.08	0.33	0.03	0.34	0.51	0.35	0.09	0.32
In3	0.26	0.6	0.56	0.5	0.54	0.09	0.41	0.12
In4	0.43	0.53	0.5	0.57	0.16	0.47	0.01	0.17
In5	0.5	0.13	0.61	0.7	0.48	0.09	0.19	0.82
In6	0.52	0.79	0.1	0.3	0.06	0.24	0.81	0.63
In7	0.63	0.3	0.29	0.13	0.31	0.12	0.6	0.23
In8	0.48	0.43	0.08	0.16	0.13	0.6	0.8	0.68

(b)

dB	Out1	Out2	Out3	Out4	Out5	Out6	Out7	Out8
In1	1.20	1.16	0.49	0.18	0.48	0.02	0.16	0.17
In2	2.25	0.57	0.07	0.56	0.13	0	0.41	0
In3	1.44	0.05	0.35	0.59	0	0.19	0.16	0.13
In4	0.05	0.25	0	0.12	0	0.08	0.35	2.36
In5	0.05	0.34	0.3	0.21	0.04	1.23	2.17	1
In6	0.72	0	0.08	0.4	0.37	2.45	0.18	0.1
In7	0	0.34	0.12	0.22	2.17	0.03	0.14	0.28
In8	0.35	0.19	0.15	2.24	0.11	0.31	0.23	0.08

Table 6. (a) Deviation of mean wavelengths from AWGR optimal resonances. (b) Standard deviation and range of mean wavelengths with respect to the AWGR peak resonances.

(a)

nm	Out1	Out2	Out3	Out4	Out5	Out6	Out7	Out8
In1	−3.4	−3.4	−3.2	0.2	−0.3	−0.2	−0.2	−0.2
In2	−3.9	−2.9	−0.1	−0.3	−0.3	0.3	0.2	0.3
In3	−3.1	0.2	−0.3	−0.2	0.0	0.1	0.6	1.0
In4	0.1	−0.1	0.0	0.2	0.0	0.2	1.5	2.7
In5	−0.1	−0.4	0.2	−0.3	0.4	1.5	2.2	0.2
In6	0.1	0.0	0.3	0.1	1.5	2.6	0.1	0.2
In7	0.0	0.1	0.6	0.6	2.7	0.0	0.8	1.0
In8	0.1	1.3	1.0	−0.7	−0.3	−0.3	−0.1	−0.2

(b)

Mean λ (nm)	S. deviation	Range (nm)	
1260.15	0.177	[−0.15,0.35]	0.5
1269.15	0.385	[−0.85,0.25]	1.1
1278.71	0.439	[−1.01,0.39]	1.4
1288.46	0.185	[−0.26,0.24]	0.5
1297.76	0.2	[−0.26,0.34]	0.6
1307.49	1.428	[−1.29,3.41]	4.7
1317.55	2.245	[−1.55,3.85]	5.4
1328.06	2.801	[−2.66,3.24]	5.9

5. Summary

We presented an O-band 8 × 8 silicon photonic integrated AWGR with a footprint of 700 × 270 μm^2 and 10 nm channel spacing, suitable for WDM interconnect routing applications. The device characterization indicated good cyclic-frequency operation with 2.5 dB best case insertion losses yielding loss non-uniformity of 3.545 dB and average channel crosstalk of 11 dB. The AWGR was evaluated also in data routing experiments for 25 Gb/s optical data signals and for all possible 8 × 8 port-combinations and routing arrangements, revealing error-free operation both when transmission at AWGR channel peak wavelength values and at 8 fixed wavelengths was employed. The maximum power penalty at a 10^{-9} BER was 0.82 dB when transmission at AWGR channel peak wavelengths was utilized and 2.45 dB when 8 fixed wavelengths equal to the AWGR mean wavelength values were employed at every AWGR input port.